Scattering from Moderately Rough Interfaces between Two Arbitrary Media

James E. Harvey, Narak Choi and Andrey Krywonos

CREOL: The College of Optics and Photonics
P. O. Box 162700, 4000 Central Florida Blvd.
The University of Central Florida
Orlando, Florida 32826

Sven Schröder
Fraunhofer IOF
Jena, Germany

Dayana H. Penalver
National Institute of Astrophysics
Optics and Electronics (INAOE)
Mexico

Abstract

The generalized Harvey-Shack (GHS) surface scatter theory has been shown to accurately predict the BRDF produced by moderately rough mirror surfaces from surface metrology data. The predicted BRDF also holds for both large incident and scattering angles. Furthermore, it provides good agreement with the classical Rayleigh-Rice theory for those surfaces that satisfy the smooth-surface criterion. The two-dimensional band-limited portion of the surface PSD contributing to scattered radiation is discussed and illustrated for arbitrary incident angles, and the corresponding relevant roughness necessary to calculate the total integrated scatter (TIS) is determined. It is shown that BRDF data measured with a large incident angle can be used to expand the range of surface roughness for which the inverse scattering problem can be solved; i.e., for which the surface PSD can be calculated from measured BRDF data. This PSD and the GHS surface scatter theory can then be used to calculate the BRDF of that surface for arbitrary incident angles and wavelengths that do not satisfy the smooth-surface criterion. Finally, the surface transfer function characterizing both the BTDF and the BRDF of a moderately rough interface separating two media of arbitrary refractive index is derived in preparation for modeling the scattering of structured thin film solar cells.

Keywords: Surface scatter, BRDF, BTDF, Surface PSD, Surface roughness.

1.0 Introduction

Surface scatter phenomena continue to be an important issue in diverse areas of science and engineering in the 21st century. In many applications it is not only the amount of scattered light, but also the angular distribution of the scattered radiation that is important. This is particularly true for four distinct types of applications: 1.) The design and analysis of stray light rejection systems required by optical systems used to view a relatively faint target in the vicinity of a much brighter object, 2.) the fabrication of "super-smooth" surfaces for high resolution X-ray and extreme ultraviolet (EUV) imaging systems, 3.) inverse scattering applications where scattered light "signatures" are used to remotely infer target characteristics, and 4.) the engineering of "enhanced roughness" to increase the efficiency of thin-film photo-voltaic solar cell applications.

For short wavelength applications, surface scatter effects from residual optical fabrication errors frequently limit the performance of imaging systems rather than geometrical aberrations or diffraction effects. Image quality predictions as degraded by surface scatter effects involve a two-step process: (*i*) first one must be able to predict the scattered light behavior, or bidirectional reflectance distribution function (BRDF),[1] from measured (or assumed) surface metrology data, and (*ii*) then one must be able to calculate the image degradation from that scattered light behavior. Several commercially-available optical design and analysis codes (ZEMAX, Code V, ASAP and FRED) have demonstrated the ability to predict the image degradation if the BRDF is provided as input. However, the required BRDF data is usually only available either through direct measurements, which is often difficult, or from calculations based on the Rayleigh-Rice scattering theory in the smooth surface limit.

The classical Rayleigh-Rice surface scatter theory (1951) is a rigorous vector treatment valid for large incident and scattered angles; however it utilizes a perturbation technique with an explicit smooth-surface approximation.[2] The

Optical System Contamination: Effects, Measurements, and Control 2010,
edited by Sharon A. Straka, Nancy Carosso, Proc. of SPIE Vol. 7794, 77940V

classical Beckmann-Kirchhoff surface scatter theory (1963) is valid for rougher surfaces, but it has an inherent paraxial or small-angle limitation.[3] Harvey and Shack (1976) developed a linear systems formulation of surface scatter phenomena in which the scattering behavior is characterized by a *surface transfer function*.[4-5] This treatment provided insight and understanding not readily gleaned from the above two theories, however, it suffered from the same paraxial limitations as the Beckmann-Kirchhoff theory. Krywonos and Harvey developed a linear systems formulation of non-paraxial scalar diffraction theory (1999) in which diffracted radiance (not intensity or irradiance) is the fundamental quantity that exhibits shift-invariant behavior in direction cosine space.[6-9] This led to the development of a unified surface scatter theory that combines the advantages of the classical Rayleigh-Rice and the Beckmann-Kirchhoff theories in that it appears to be valid for both smooth and moderately rough surfaces and at arbitrary incident and scattered angles.[10-11]

2.0 The Generalized Harvey-Shack Surface Scatter Theory

Figure 1 illustrates the optical path difference introduced when a ray incident upon a scattering surface at an arbitrary incident angle, θ_i, is scattered at an arbitrarily large angle, θ_s. It is obvious from examining the figure that the optical path difference introduced upon reflection depends not just on the surface height and incident (or specular) angle, but also on the scattering angle θ_s. The OPD can be written as

$$OPD = (\cos\theta_i + \cos\theta_s)\, h(\hat{x}, \hat{y})\,. \tag{1}$$

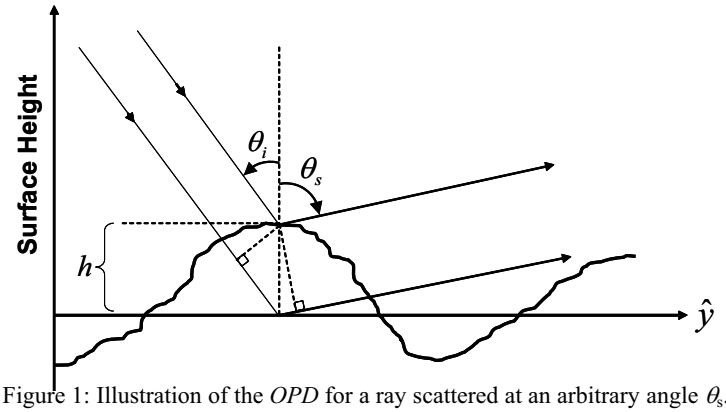

Figure 1: Illustration of the *OPD* for a ray scattered at an arbitrary angle θ_s.

The random phase induced upon the reflected wavefront for light scattered at an arbitrary angle is thus given by the following expression

$$\phi(\hat{x}, \hat{y}) = (2\pi/\lambda)\, OPD = 2\pi(\gamma_i + \gamma_s)\, \hat{h}(\hat{x}, \hat{y})\,. \tag{2}$$

where

$$\gamma_i = \cos\theta_i \text{ and } \gamma_s = \cos\theta_s\,. \tag{3}$$

Note that a scaled coordinate system has been used in which the spatial variables are normalized by the wavelength of the light ($\hat{x} = x/\lambda, \hat{y} = y/\lambda$, etc.). The reciprocal variables α and β are thus the *direction cosines* of the propagation vectors of the angular spectrum of plane waves discussed by Ratcliff,[12] Goodman,[13] and Gaskill.[14]

Following the derivation of the original Harvey-Shack theory[4,10] (similar to the derivation of the optical transfer function in modern image formation theory) we find that the following two-parameter family of surface transfer functions

$$H_s(\hat{x}, \hat{y}; \gamma_i, \gamma_s) = \exp\left\{-\left[2\pi\hat{\sigma}_{rel}(\gamma_i + \gamma_s)\right]^2\left[1 - C_s(\hat{x}, \hat{y})/\sigma_{rel}^2\right]\right\} \tag{4}$$

is required to characterize the scattering behavior for arbitrary incident and scattering angles;[10-11] i.e., a separate surface transfer function is required for each incident angle *and* each scattering angle. $C_s(\hat{x}, \hat{y})$ is the surface autocovariance function, and σ_{rel} is the *band-limited relevant rms roughness* that will be discussed in detail in Section 3.

The BRDF is then obtained by Fourier transforming the surface transfer function and multiplying by the reflectance of the surface[10-11]

$$BRDF = Q\,\mathcal{F}\{H_s(\hat{x},\hat{y};\gamma_i,\gamma_s\} \; . \tag{5}$$

Note that we have quasi-vectorized our scalar treatment of surface scatter phenomena by substituting the polarization reflectance, Q, for the scalar reflectance, R.[11]

3.0 The Relevant Surface Characteristics

The well-known Rayleigh-Rice surface scatter theory results in the following expression for the BRDF in terms of the two-dimensional surface power spectral density (PSD) function[15]

$$BRDF = \frac{16\pi^2}{\lambda^4}\cos\theta_i \cos\theta_s \, Q \, PSD(f_x, f_y) \tag{6}$$

where the surface PSD is expressed in terms of the sample spatial frequencies provided by the hemispherical grating equation

$$f_x = \frac{\sin\theta_s \cos\phi_s - \sin\theta_i}{\lambda} \text{ and } f_y = \frac{\sin\theta_s \sin\phi_s}{\lambda} \quad . \tag{7}$$

For isotropic roughness, the surface PSD is rotationally symmetric, and for normal incidence, spatial frequencies greater than 1/λ do not produce scatter light (corresponding diffracted order is scattered at an angle greater than 90 degrees). Those spatial frequencies greater than 1/λ instead produce evanescent (imaginary) waves that do not result in radiant power being scattered from the specular beam; i.e.; spatial frequencies greater than 1/λ are completely *irrelevant* with regard to scattered light. There has thus been a strong emphasis placed upon the necessity for including appropriate spatial frequency band-limits whenever one measures or specifies a particular rms surface roughness.[15-16] Figure 2 illustrates the relevant band-limited portion of the surface PSD for an isotropically rough surface with normally-incident light.

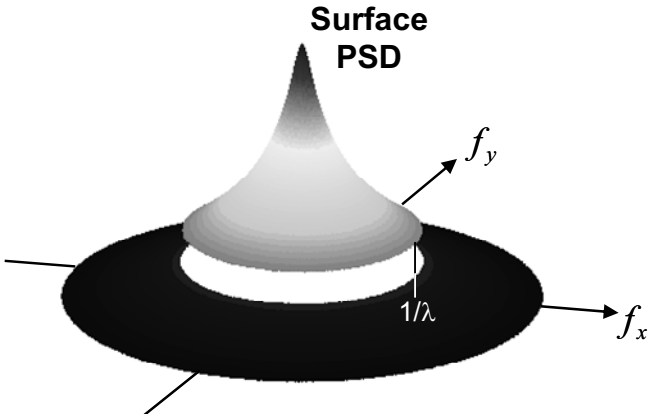

Figure 2. Illustration of the rotationally symmetric surface PSD resulting from a surface exhibiting isotropic roughness. For normally-incident light, the relevant portion of the PSD is that portion bounded by a circle of radius 1/λ.

The relevant (or effective) roughness, σ_{rel}, is given by the square root of the integral under the relevant portion of the surface PSD and is thus a function of wavelength. For isotropic roughness:

$$\sigma_{rel}(\lambda) = \sqrt{2\pi \int_{f=0}^{1/\lambda} PSD(f)\, f \, df \, d\phi} \quad . \tag{8}$$

For an arbitrary incident angle, θ_i, the 2-dimensional boundary of the appropriate band-limited portion of the surface PSD is illustrated in Figure 3(a). It is that portion of the surface PSD bounded by a circle of radius 1/λ whose center is shifted to a spatial frequency given by

$$f_o = \frac{\sin\theta_o}{\lambda} \quad , \quad \theta_o = -\theta_i \quad . \tag{9}$$

The corresponding relevant roughness, σ_{rel}, is given by the volume under the relevant portion of the surface PSD illustrated in Figure 3(b). It is thus calculated by the following integral

$$\sigma_{rel}(\lambda) = \sqrt{\int_{-1/\lambda+f_o}^{1/\lambda+f_o} \int_{-\sqrt{1/\lambda^2-(f_x-f_o)^2}}^{\sqrt{1/\lambda^2-(f_x-f_o)^2}} PSD\left(f_x, f_y\right) df_x \, df_y} \, . \tag{10}$$

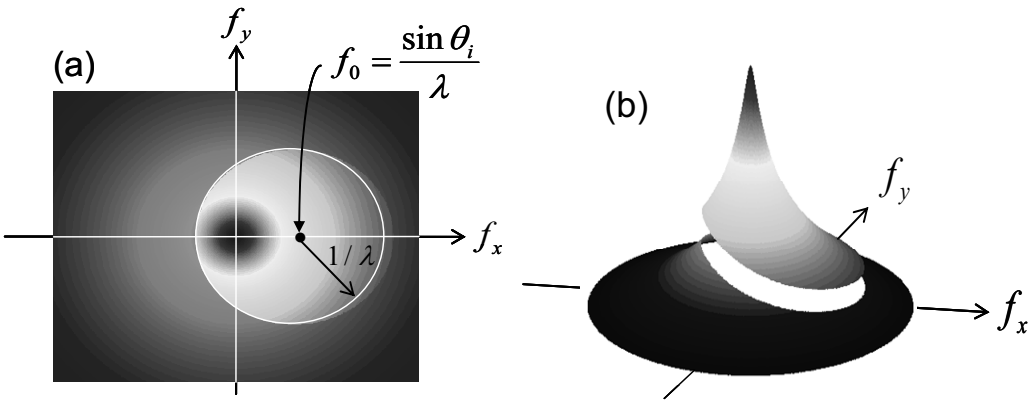

Figure 3. (a) Illustration of the 2-dimensional boundary of the appropriate band-limited portion of the surface PSD for an arbitrary incident angle, θ_i. (b) illustration of the relevant portion of the surface PSD, whose integral yields the relevant rms surface roughness.

Since perfectly smooth mirror surfaces don't exist (there is always some residual surface roughness), the reflected light consists of a somewhat diminished specularly reflected beam and an associated scattered light component. It is the above relevant roughness, σ_{rel}, that determines the relative amount of light in these two components. The fraction of the total reflected radiant power contained in the specular component after reflection from a moderately rough surface is given by

$$A = \exp[-(4\pi\cos\theta_i \, \sigma_{rel}/\lambda)^2] \tag{11}$$

and the fraction of the total reflected radiant power that is scattered out of the specular beam, or total integrated scatter (TIS), is given by

$$B = TIS = 1 - \exp[-(4\pi\cos\theta_i \, \sigma_{rel}/\lambda)^2] \quad . \tag{12}$$

Clearly the sum of these two quantities equals unity ($A + B = 1$).

4.0 Large Incident Angles and the Inverse Scattering Problem

Surface scatter of electromagnetic radiation is not caused directly by surface roughness, but rather by the effect of the *phase variation* induced upon the transmitted or reflected wavefront as it propagates; i.e., surface scatter is a *diffraction phenomena* caused by the *propagation process*. As such, surface scatter is strongly affected by the propagating wavelength, the statistical characteristics of the surface (the surface PSD or the surface autocovariance function), the angle of incidence, and the refractive index of the media both before and after the interface or surface encountered.

The smooth-surface criterion must be satisfied to perform the inverse scattering problem of predicting surface characteristics from BRDF Measurements.[15] From Eq.(6) we can then write

$$PSD(f_x, f_y) = \frac{\lambda^4}{16\pi^2} \frac{BRDF}{Q \cos\theta_i \cos\theta_s} \quad . \tag{13}$$

The smooth-surface criterion for the Rayleigh-Rice surface scatter theory is written below in Eq.(14).[15-16] This roughness parameter is called "*g*" by Beckmann.[3]

$$g = (4\pi\sigma_{rel} \cos\theta_i / \lambda)^2 << 1 \quad . \tag{14}$$

This could just as well be called the long wavelength criterion, or the large incident angle criterion. In fact, this expression suggests that a *large incident angle can compensate for a moderately rough surface*.

Figure 4 shows several BRDF curves measured from the back side of a silicon wafer by John Stover of The Scatter Works in Tucson, AZ. Note that measurements were made at four different incident angles from 5 to 80 degrees. This was a rather rough surface that did not produce even a faint reflection of one's face when observed at normal incidence.

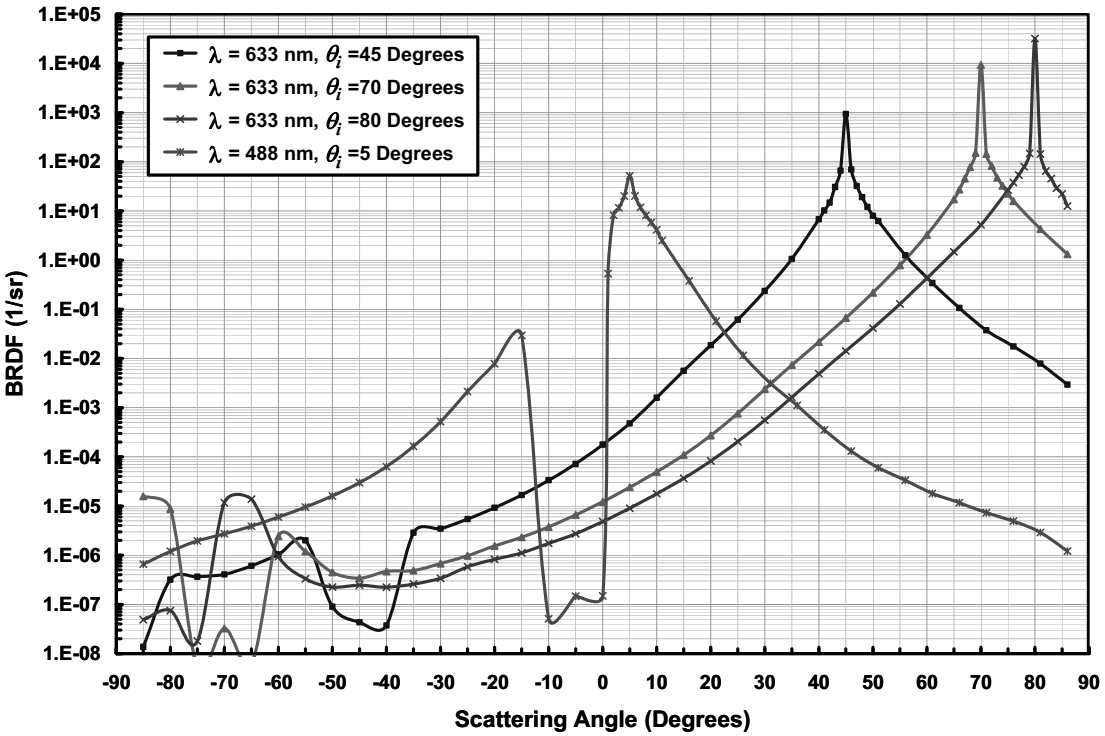

Figure 4. Four different BRDF scans were made from the backside of a silicon wafer. Variations in wavelength and incident angle were used to vary the apparent "roughness" of the wafer as determined by the Rayleigh criterion.

However, because of the strong effect of the incident angle upon the value of the roughness parameter in Eq.(14), the backscattered BRDF profile measured at an incident angle of 80 degrees was used to predict the surface PSD from Eq.(13). The resulting surface PSD is illustrated in Figure 5 along with a fitting function made up of the sum of five ABC, or K-correlation functions.[15-18] The appropriate integral as discussed in the previous section was then calculated to determine the relevant roughness for each wavelength and incident angle represented by the four BRDF plots. The total, or intrinsic, roughness of the surface as well as the relevant roughness and the corresponding value of the roughness parameter, *g*, are also indicated in Figure 5 for each of the BRDF curves.

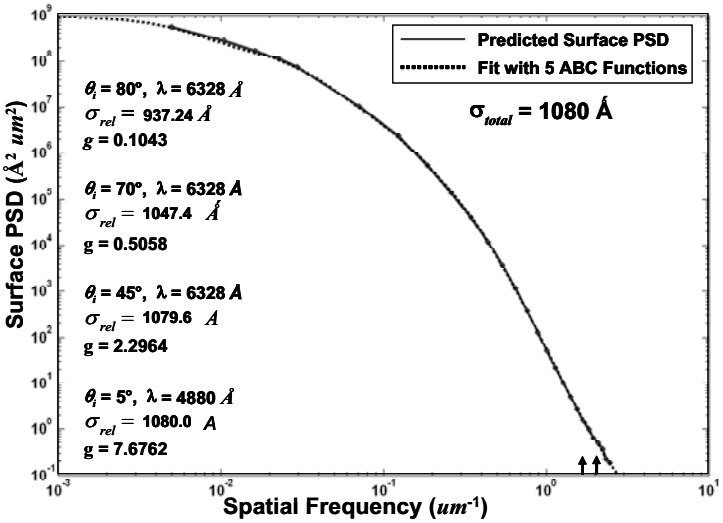

Figure 5. The surface PSD calculated from the 80° BRDF scan is fit with the sum of five ABC functions. That fitting function is then integrated to obtain the total roughness and the relevant roughness and the value of the roughness parameter for each of apparent "roughness" of the wafer as determined by the Rayleigh criterion.

For the incident angles and wavelengths represented by the four BRDF curves, the roughness parameter, g, varies in magnitude from $0.1043 < g < 7.6762$; i.e., from quite smooth (more than half of the reflected light in the specular beam) to very rough (99.9% of the reflected light scattered).

Since $g \sim 0.1$ for the BRDF profile measured at an incident angle of 80 degrees, the smooth-surface criterion can be considered to be satisfied and we have a high level of confidence in the surface PSD predicted from Eq.(13). We can now use that surface PSD to predict BRDF profiles at arbitrary incident angles and wavelengths. Figure 6 shows the comparison of BRDF profiles predicted with both the GHS and the Rayleigh-Rice surface scatter theories with the experimental measurements for the 5°, 45° and 70° incident angles previously shown.

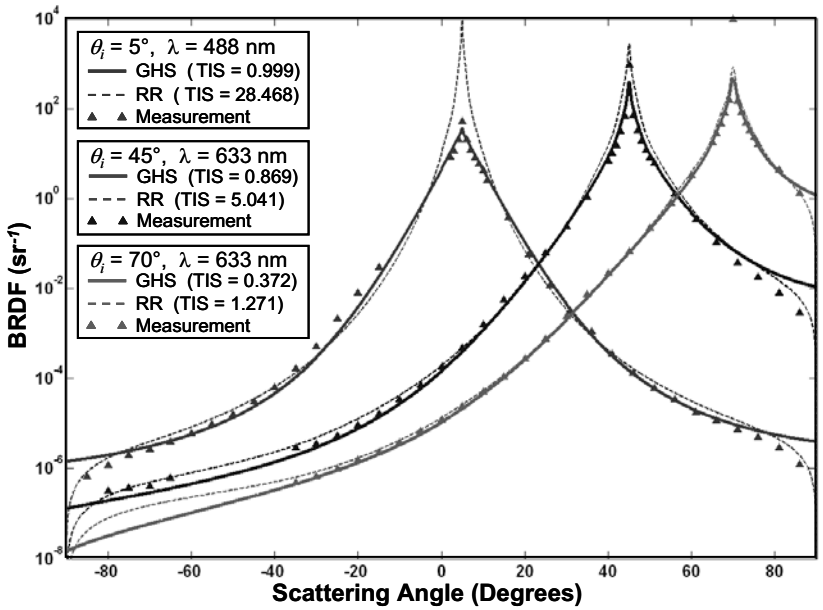

Figure 6. These curves demonstrate that the incident angle can be increased to satisfy the smooth-surface criterion required to solve the inverse scattering problem of determining surface characteristics from scattered light measurements. The resulting surface PSD can then be used to predict the BRDF of moderately rough surfaces at arbitrary incident angles and wavelengths.

The predictions from the GHS surface scatter theory agree with the measured data quite well, even for the 5° incident angle case, whereas the BRDF predicted by the Rayleigh-Rice theory is more than two orders of magnitude too high near the specular beam. The TIS values calculated by numerical integration of the BRDF predicted from both the GHS and the Rayleigh-Rice theories are also indicated on Figure 6. The unrealistically large TIS values predicted by the Rayleigh-Rice theory are merely evidence of the smooth-surface approximation inherent in that theory. These curves provide convincing evidence that the incident angle can be varied to satisfy the smooth surface criterion so that the inverse scattering problem can be solved, even for what are usually considered to be rough surfaces.

5.0 The Surface Transfer Function for a Moderately Rough Interface between Two Arbitrary Media

Much has been written about the scattering properties of mirror surfaces since the scattered light can severely degrade the optical performance of imaging systems. A more general situation arises when we have a moderately rough interface separating two dielectric media characterized by arbitrary refractive indices as illustrated in Figure 7.

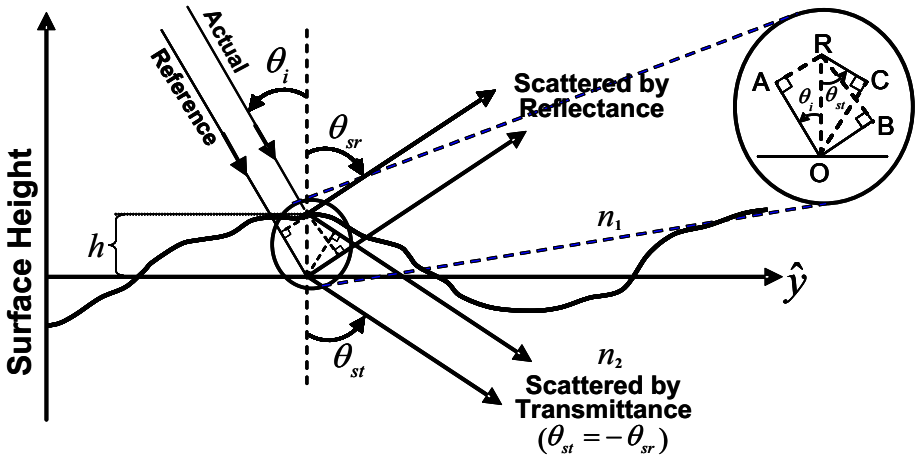

Figure 7. Illustration of scattering in both reflection and transmission from a moderately rough interface separating two dielectric media characterized by arbitrary refractive indices.

The optical path difference (OPD) between a reference ray and a ray scattered at an arbitrary angle is defined as the difference between the actual and the reference optical path length (OPL)

$$OPD = OPL_{actual} - OPL_{reference} \quad . \tag{15}$$

For an arbitrary incident angle, θ_i, and an arbitrary scattering angle, θ_s, it is clear from the inset that the OPD for reflectance and transmittance is given by

$$OPD_r = -\left(n_1 AO + n_2 OB\right) \tag{16}$$

and

$$OPD_t = -\left(n_1 AO - n_2 RC\right) \tag{17}$$

respectively. Note that the reflected scattering angle, θ_{sr}, and the transmitted scattering angle, θ_{st}, are of equal magnitude but opposite in sign. Since the refractive index after reflectance is always taken to be the negative of the refractive index before reflection, the following equation holds for both cases where we have dropped the *r* and *t* designation on the scattering angle

$$OPD = -h\left(n_1 \cos\theta_i - n_2 \cos\theta_s\right) \quad . \tag{18}$$

For a plane wavefront incident, the phase variation induced upon either the reflected or transmitted wavefront is thus given by

$$\phi(\hat{x},\hat{y}) \;=\; (2\pi/\lambda)\, OPD = -2\pi\left(n_1\cos\theta_i - n_2\cos\theta_s\right)\hat{h}(\hat{x},\hat{y}) \tag{19}$$

where θ_i is the incident angle, θ_s is the scattered angle, n_1 and n_2 are the refractive indices on the incident and the opposite side of the interface, respectively (set $n_1 = -n_2$ for reflection).

Clearly there will be both a BRDF and a bidirectional transmittance distribution function (BTDF) produced when the incident wave strikes the interface between the two media as illustrated schematically in Figure 8. Both the BRDF and the BTDF will consist of a specular beam and a scattering function. The total reflectance, R, will be given by the Fresnel reflectance equations (indicated in the figure for the special case of normal incidence).

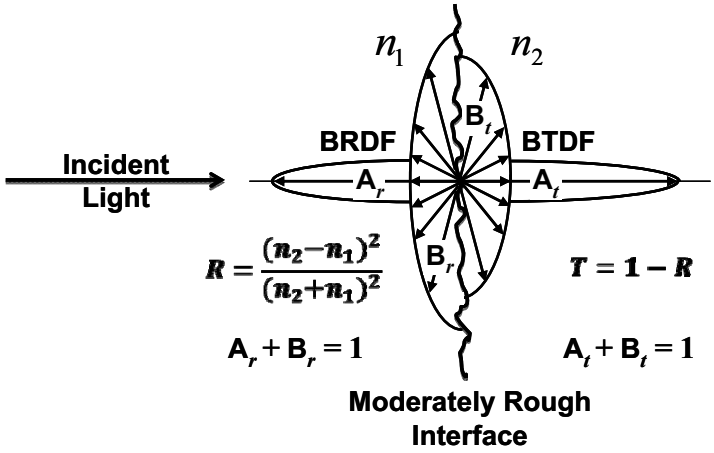

Figure 8. Schematic illustration of the BRDF and BTDF produced from a moderately rough interface separating two dielectric media characterized by arbitrary refractive indices.

Again following the derivation of the original Harvey-Shack theory[4,10] (similar to the derivation of the optical transfer function in modern image formation theory) we obtain that the following two-parameter family of surface transfer functions that characterizes both the BRDF and the BTDF (set $n_1 = -n_2$ for BRDF).

$$H_s(\hat{x},\hat{y};\gamma_i,\gamma_s) \;=\; \exp\left\{-\left[2\pi\hat{\sigma}_{rel}(n_1\gamma_i - n_2\gamma_s)\right]^2\left[1 - C_s(\hat{x},\hat{y})/\sigma_{rel}^2\right]\right\} \;. \tag{20}$$

6.0 Enhanced Roughness for Increasing the Efficiency of Thin-Film Photovoltaic Solar Cells

There is considerable interest in the possibility of significantly increasing the efficiency of thin-film photovoltaic silicon solar cells by utilizing enhanced roughness on the TCO-Si interface as shown in Figure 9.[19-21] The necessary transmissive conductive oxide (TCO) layer is deposited onto a glass substrate. The enhanced roughness interface between the TCO and silicon might be produced by acid-etching the TCO surface before depositing a thin-film (~ 600nm) layer of silicon. A reflective coating would probably then be deposited on the back side of the silicon.

The GHS surface scatter theory discussed above might serve as a valuable tool in evaluating the effectiveness of the enhanced roughness in improving the efficiency of such a thin-film silicon solar cell.

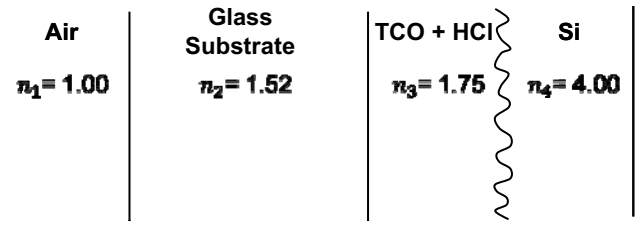

Figure 9. Typical configuration for an enhanced roughness thin-film silicon solar cell for photovoltaic applications.

Roughened TCO films were produced at the Fraunhofer IOF for preliminary evaluation on glass substrates using pulsed DC magnetron sputtering and subsequent chemical etching. Roughness analysis was performed by combining Atomic Force Microscopy and Phase-Shift-Interferometry as described in Reference 22. Figure 10 shows the measured surface PSDs of the glass substrate, the TCO surface before etching and the TCO coating after acid etching.

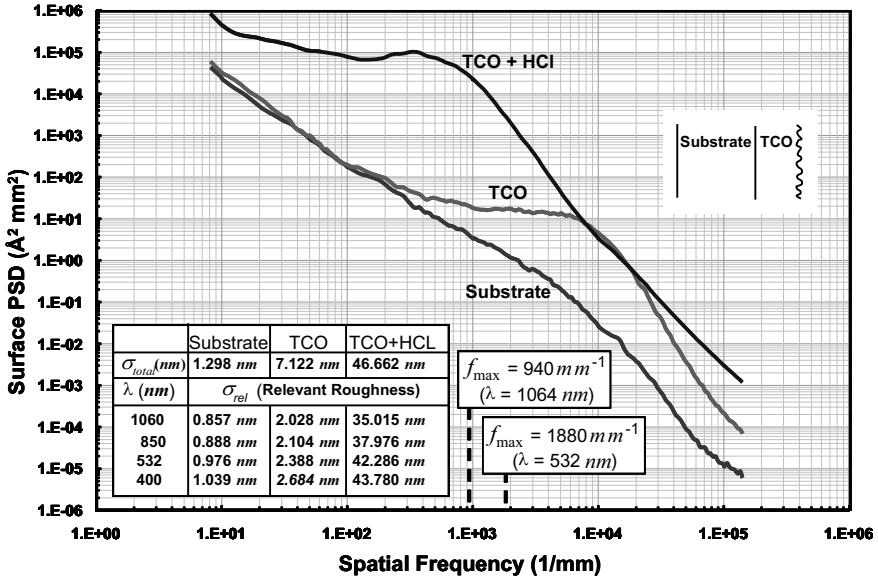

Figure 10. Measured surface PSDs of a preliminary TCO surface for a thin-film silicon solar cell.

The maximum relevant spatial frequency is indicated on the graph for wavelengths of 1064 nm and 532 nm at normal incidence. The relevant roughness of the surfaces have also been calculated and tabulated in Figure 10 for several wavelengths spanning the solar spectrum.

The BTDF produced by the TCO + HCl surface has been calculated with the GHS surface scatter theory as described Reference 18. Figure 11 shows a comparison of these predictions with BTDF measurements made at Fraunhofer IOF at a wavelength of 1064 nm using the instrumentation described in Reference 23. The predicted BTDF was adjusted for the reflection losses of the air-glass, glass-TCO and the TCO-air interface. Also the size and shape of the specular beam of the predicted BTDF was calculated from the size of the incident beam and detector characteristics of the scatterometer used in making the experimental BTDF measurements.

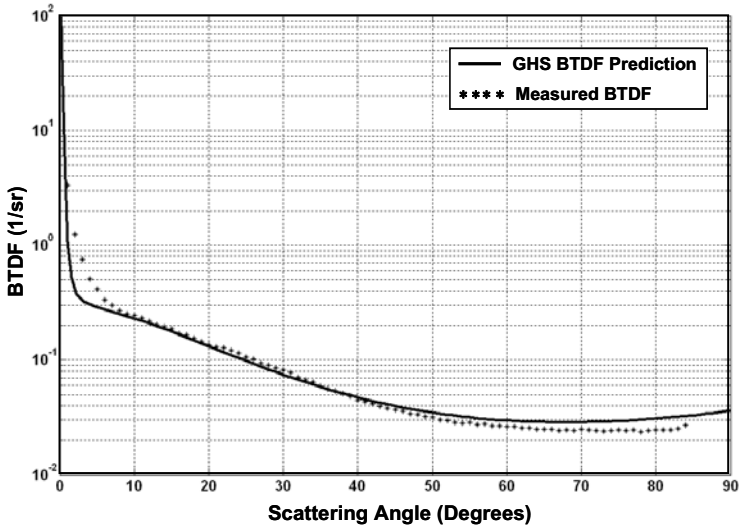

Figure 11. Comparison of the BTDF predicted with the GHS surface scatter theory with measured BTDF data.

7.0 Summary and Conclusions

The generalized Harvey-Shack (GHS) surface scatter theory that is valid for both moderately rough surfaces and large incident and scattered angles was briefly reviewed. We then discussed in detail the relevant surface characteristics (2-D band-limited surface PSD) with regard to surface scatter behavior. In particular we described how to calculate the relevant, or effective rms roughness that determines the total integrated scatter (TIS).

We re-iterated the well-known fact that the inverse scattering problem requires that the smooth-surface criterion be satisfied. It was suggested that BRDF measurements made at a large incident angle can compensate for a moderately rough surface in satisfying the smooth-surface criterion. A BRDF profile measured at an 80° incident angle was then used to predict the surface PSD for a moderately rough surface. The GHS surface scatter theory then used that predicted surface PSD to calculate the BRDF at a variety of arbitrary incident angles and wavelengths. Those predicted BRDFs were validated with experimental measurements.

Finally we derived a surface transfer function for an arbitrarily rough interface between two arbitrary media. This surface transfer function allows the GHS surface scatter theory to predict both the BRDF and the BTDF. This new generalization allows the GHS surface scatter theory to be applied to the problem of evaluating the effectiveness of enhanced roughness in improving the efficiency of thin-film silicon solar cells. Excellent agreement between predicted and measured BTDFs for an acid-etched TCO surface was obtained.

8.0 Acknowledgements

The contributions of Angela Duparré, Kevin Füchsel, Tobias Herffurth, and Luise Coriand of the Fraunhofer IOF for their contributions to the investigations of TCO films are gratefully acknowledged.

9.0 References

1. S. O. Rice, “Reflection of electromagnetic waves from slightly rough surfaces,” *Commun. Pure Appl. Math.* **4**, 351 (1951).
2. P. Beckmann and A. Spizzichino, *The Scattering of Electromagnetic Waves from Rough Surfaces*, Pergamon Press, New York (1963).
3. J. E. Harvey, *Light-scattering Characteristics of Optical Surfaces*, Ph.D. Dissertation, University of Arizona (1976).
4. J. E. Harvey, “Surface Scatter Phenomena: A Linear, Shift-invariant Process”, in *Scatter from Optical Components*, J. C. Stover, ed., Proc. SPIE **1165**, 87-99 (1989).
5. J. E. Harvey, C. L. Vernold, A. Krywonos, and P. L. Thompson, “Diffracted Radiance: A Fundamental Quantity in Non-Paraxial Scalar Diffraction Theory”, Appl. Opt. **38**, 6469-6481 (November 1999).
6. J. E. Harvey, C. L. Vernold, A. Krywonos, and P. L. Thompson, “Diffracted Radiance: A Fundamental Quantity in Non-Paraxial Scalar Diffraction Theory: Eratta”, Appl. Opt. **39**, 6374-6375 (Dec. 1, 2000).
7. J. E. Harvey and C. L. Vernold, “Description of Diffraction Grating Behavior in Direction Cosine Space”, Appl. Opt. **37**, 8158-8160 (Dec. 1, 1998).
8. J. E. Harvey, A. Krywonos, and Dijana Bogunovic, “Non-paraxial Scalar Treatment of Sinusoidal Phase Gratings”, scheduled for publication in JOSA A (April 2006).
9. A. Krywonos, *Predicting Surface Scatter using a Linear Systems Formulation of Non-paraxial Scalar Diffraction*, Ph.D. Dissertation, College of Optics and Photonics, University of Central Florida (2006).
10. J. E. Harvey, A. Krywonos, and J. C. Stover “Unified Scatter Model for Rough Surfaces at Large Incident and Scattered Angles”, **Invited Paper** presented at SPIE’s International Symposium on Optics and Photonics, San Diego, CA, August 2007; published in Proc. SPIE **6672-12** (August 2007).
11. J. A. Ratcliff, “Some Aspects of Diffraction Theory and Their Application to the Ionosphere”, in *Reports of Progress in Physics*, edited by A. C. Strickland (The Physical Society, London, 1956), Vol. XIX.
12. J. W. Goodman, *Introduction to Fourier Optics*, 2nd Ed., McGraw-Hill, New York (1996).

13. J. D. Gaskill, *Linear Systems, Fourier Transforms, and Optics*, Wiley, New York (1978).
14. F. E. Nicodemus, "Reflectance Nomenclature and Directional Reflectance and Emissivity", Appl. Opt. **9**, 1474-5 (1970).
15. J. C. Stover, *Optical Scattering, Measurement and Analysis*, 2nd Edition, SPIE Press, Bellingham, WA (1995).
16. E. L. Church and P. Z. Takacs, "Light Scattering from Non-Gaussian Surfaces", Proc. SPIE 2541, 91-107 (1995).
17. M. G. Dittman, "K-correlation power spectral density & surface scatter model", Proc. SPIE 6291, 62910R (2006).
18. J. E. Harvey N. Choi, and A. Krywonos, "Calculating BRDFs from Surface PSDs for Moderately Rough Optical Surfaces", Proc. SPIE **7426-42** (2009).
19. S. Fay, S. Dubail, U. Kroll, J. Meier, Y. Ziegler and A. Shah, "Light Trapping Enhancement for Thin-film Silicon Solar Cells by Roughness Improvement of the ZnC Front TCO", Proc. 16th EU-PVSEC, 361-364 Glasgow, (2000).
20. D. Domine, F. J. Haug, C. Battaglia and C. Ballif, "Modeling of light scattering from micro- and nanotextured surfaces", Journal of Applied Physics **107**, 044504 (2010).
21. S. Schröder, A. Duparré, K. Füchsel, N. Kaiser, A. Tünnermann, J. E. Harvey, "Scattering of Roughened TCO Films—Modeling and Measurement", presented at OSA Topical Meeting on Optical Interference Coatings, Tucson, AZ, June 7-9, 2010; Technical Digest – CD-ROM.
22. A. Duparré, J. Ferre-Borrull, S. Gliech, G. Notni, J. Steinert, J. M. Bennett, "Surface Characterization Techniques for Determining the Root-Mean-Square Roughness and Power Spectral Densities of Optical Components," Appl. Opt. 41, 154-171 (2002)
23. S. Schröder, T. Herffurth, H. Blaschke, A. Duparré, "Angle Resolved Scattering: An Effective Method for Characterizing Thin Film Coatings", submitted for publication in Applied Optics (July 2010).